



## PSI–LHCI of *Chlamydomonas reinhardtii*: Increasing the absorption cross section without losing efficiency



Clotilde Le Quiniou, Lijin Tian, Bartłomiej Drop, Emilie Wientjes, Ivo H.M. van Stokkum, Bart van Oort, Roberta Croce\*

Department of Physics and Astronomy, Faculty of Sciences, VU University Amsterdam, Institute for Lasers, Life and Biophotonics Amsterdam, LaserLab Amsterdam, De Boelelaan 1081, 1081 HV Amsterdam, The Netherlands

### ARTICLE INFO

#### Article history:

Received 2 December 2014  
Received in revised form 28 January 2015  
Accepted 2 February 2015  
Available online 10 February 2015

#### Keywords:

Photosystem I  
Light-harvesting complex I  
*Chlamydomonas reinhardtii*  
Red forms  
Time-resolved fluorescence  
Trapping efficiency

### ABSTRACT

Photosystem I (PSI) is an essential component of photosynthetic membranes. Despite the high sequence and structural homologies, its absorption properties differ substantially in algae, plants and cyanobacteria. In particular it is characterized by the presence of low-energy chlorophylls (red forms), the number and the energy of which vary in different organisms. The PSI–LHCI (PSI–light harvesting complex I) complex of the green alga *Chlamydomonas reinhardtii* (*C.r.*) is significantly larger than that of plants, containing five additional light-harvesting complexes (together binding  $\approx 65$  chlorophylls), and contains red forms with higher energy than plants. To understand how these differences influence excitation energy transfer and trapping in the system, we studied two PSI–LHCI *C.r.* particles, differing in antenna size and red-form content, using time-resolved fluorescence and compared them to plant PSI–LHCI. The excited state kinetics in *C.r.* shows the same average lifetime (50 ps) as in plants suggesting that the effect of antenna enlargement is compensated by higher energy red forms. The system equilibrates very fast, indicating that all Lhcas are well-connected, despite their long distance to the core. The differences between *C.r.* PSI–LHCI with and without Lhca2 and Lhca9 show that these Lhcas bind red forms, although not the red-most. The red-most forms are in (or functionally close to) other Lhcas and slow down the trapping, but hardly affect the quantum efficiency, which remains as high as 97% even in a complex that contains 235 chlorophylls.

© 2015 The Authors. Published by Elsevier B.V. This is an open access article under the CC BY-NC-ND license (<http://creativecommons.org/licenses/by-nc-nd/4.0/>).

### 1. Introduction

Photosynthesis provides energy for nearly all life on Earth. In the first step of photosynthesis, light is harvested by photosystem (PS) I and II, which are multi-protein complexes embedded in the thylakoid membrane. Their light-harvesting system is composed of a large number of pigments coordinated by proteins. In both PSs the excitation energy is efficiently transferred to the reaction center (RC) where charge separation (CS) occurs [1]. In eukaryotic organisms, as the unicellular green alga *Chlamydomonas reinhardtii* (*C.r.*), PSI can be divided in two main parts: the core and the peripheral antennas. The core complex is composed of 14 protein subunits (PsaA–PsaL, PsaN and PsaO), together binding  $\approx 100$  chlorophylls (Chls) and  $\approx 20$  carotenoids (Cars) [2].

**Abbreviations:** PSI, Photosystem I; LHCI, Lhca, light-harvesting complex I; RC, reaction center; CS, charge separation; *C.r.*, *Chlamydomonas reinhardtii*; Chl, chlorophylls; Car, carotenoids; *A.t.*, *Arabidopsis thaliana*; EET, excitation energy transfer; PMS, phenazine metasulfate; RT, room temperature; CD, circular-dichroism; TR, time range; DAS, Decay Associated Spectra; EAS, Evolution Associated Spectra; SAS, Species Associated Spectra

\* Corresponding author at: Department of Physics and Astronomy, Faculty of Sciences, VU University Amsterdam, De Boelelaan 1081, 1081 HV Amsterdam, The Netherlands. Tel.: +31 205986310.

E-mail address: [r.croce@vu.nl](mailto:r.croce@vu.nl) (R. Croce).

The core coordinates only Chls *a*, a few of which constitute the RC. The peripheral antenna, called the light-harvesting complex I (LHCI) or Lhcas, is composed of different Lhca gene products that in addition to Chls *a* and Car, coordinate Chls *b* ([3,4]). In the following we will refer to the PSI supercomplex, composed of the core and peripheral antennas, as PSI–LHCI.

The PSI core complex is very similar among oxygenic photosynthetic organisms [5]. Highly conserved structures of PSI core have been observed for cyanobacteria ([2,6]) and higher plants ([7,8]). The primary structure of the core proteins of *C.r.* shows high homology with that of plants and cyanobacteria ([9,10]), suggesting a conserved structure. At variance with the core, the peripheral antenna of higher plants and of *C.r.* shows major differences in the number of genes ([11–13]) and in the biochemical/spectroscopic properties of the complexes [14]. PSI–LHCI of *C.r.* contains nine Lhca proteins (Lhca1–9), located on one side of the core, forming two parallel concentric half rings [15], by contrast to higher plants PSI–LHCI that is formed of one half ring made of only four Lhca proteins ([16,7]).

Another major difference between PSI–LHCI of *C.r.*, higher plant and cyanobacteria is the content of red forms. These red forms are Chls with red-shifted absorption and emission, a large Stokes shift and a large bandwidth compared to bulk Chls (e.g. [17–20]). The red forms

dominate the low temperature fluorescence emission and are responsible for the 712–717 nm emission in *C.r.* cells and isolated *C.r.* PSI–LHCI ([21–24,15]). This maximum is at higher energy than that of *Arabidopsis thaliana* (*A.t.*) PSI–LHCI (maximum at 735 nm, [25]) and of most cyanobacteria PSI trimers (e.g. 760 nm in *Arthrospira platensis*, previously called *Spirulina platensis*, [26,27]). Red forms can be associated with the core and/or with the peripheral antenna of PSI–LHCI. Interestingly, despite the high structural homology of PSI core complexes, the red forms present in the core of different organisms can substantially differ in energy [27]. In plants the red-most forms are associated with Lhca3 and Lhca4 ([28,29]), while the core emits at 720 nm [30]. In *C.r.* red forms are proposed to be associated with both core and peripheral antennas ([23,31,24,32–35]). More recently, an in vitro study of *C.r.* Lhcas has shown that Lhca2, Lhca4 and Lhca9 display the most red-shifted emission [14]. An oligomer of Lhcas, lacking Lhca2, Lhca3 and Lhca9, isolated from a PSI core-minus mutant, has an emission maximum at 708 nm at 77 K [33], supporting the attribution of the red-most forms to Lhca2 and Lhca9. Nevertheless, the loss of Lhca2 and Lhca9 did not lead to a blue shift of the emission maximum of PSI–LHCI [15], indicating that those complexes are not the (only) responsible for the red-most emission.

Excitation energy transfer (EET) from the red forms to the RC needs to be thermally activated [36] and in higher plants and cyanobacteria, the red forms slow down the trapping kinetics ([27,37]). The average decay time is 23 ps for the PSI core of higher plants (e.g. [38,37]) and ranges from 23 ps to  $\approx$  37 ps in different cyanobacteria species with increasing red forms content (e.g. [27]). In *A.t.* PSI–LHCI the “blue” Lhca complexes (Lhca1 and Lhca2) transfer excitation energy to the core four times faster than the “red” Lhca (Lhca3 and Lhca4) [37].

Several time-resolved measurements have been performed on isolated PSI–LHCI of *C.r.* ([39,35,40,41]) but they have led to different results. This is probably due to differences in the protein composition of the preparations because *C.r.* PSI–LHCI easily loses part of the Lhcas [15]. Furthermore, in these measurements, phenazine methosulfate (PMS) was used to maintain the PSI RC in its open state, whereas PMS was recently shown to quench chlorophyll emission [42]. Since it was also demonstrated that the trapping kinetics of PSI in open and closed states differ for less than 4% [42], all the measurements reported here are performed in the absence of PMS or other reducing agents. In this work we measure the fluorescence decay kinetics of two biochemically and structurally well characterized *C.r.* PSI–LHCI complexes obtained in homogeneous preparations [15]. These two PSI particles have different antenna composition containing either nine Lhcas (named the “Full PSI–LHCI” in the following) or seven Lhcas (named the “Small PSI–LHCI” in the following) lacking two red-form containing antennas Lhca2 and Lhca9. Comparing these particles allows us to study how red forms and antenna size influence EET and trapping kinetics of *C.r.* PSI–LHCI.

## 2. Materials and methods

### 2.1. Sample preparation

PSI–LHCI particles from *C.r.* were prepared as in Drop et al. (2011) [15]. Small PSI–LHCI was prepared by solubilizing Full PSI–LHCI (final chlorophyll concentration of 0.2 mg/ml) with 0.5% n-Dodecyl- $\beta$ -D-maltoside ( $\beta$ -DM) and 0.2% Zwittergent 3–16 (CalbioChem), and centrifuged overnight (41,000 rpm, 17 h at 4 °C). After centrifugation, two fractions were collected: the upper one was Small PSI–LHCI obtained after solubilization and the lower one was Full PSI–LHCI (still not solubilized). Determination of the Chl *a*, Chl *b* and Car content in the *C.r.* PSI–LHCI particles (Table 1) requires several estimations. We estimate the total number of Chls in *C.r.* by adding the total number of Chls found in higher plants PSI–LHCI (170, [7]) with the total number of Chls in the additional Lhcas found in *C.r.* PSI–LHCI particles [15]. For that, we assume the total number of Chls per Lhca to be 13, between the 10–12

**Table 1**

Estimation of the number of Chls and Cars in different PSI–LHCI supercomplexes (see Materials and methods).

	Cyanobacteria core PSI [2]	<i>A.t.</i> PSI–LHCI	<i>C.r.</i> Small PSI–LHCI	<i>C.r.</i> Full PSI–LHCI
Number of Lhcas		4	7	9
Chls <i>a</i> + Chls <i>b</i>		170	209	235
Chls <i>a</i> / Chls <i>b</i>		9.7 $\pm$ 0.4 [25]	4.8 $\pm$ 0.2 [15]	4.4 $\pm$ 0.1 [15]
Chls <i>a</i>	100	154	173	191
Chls <i>b</i>	0	16	36	44
Carotenoids	22	35	46	52

estimated in purified Lhca ([43,44]) and the 14–17 found in the crystal structure [8]. The Chl *a/b* ratio of the PSI–LHCI reported in [15] was obtained by fitting the absorption spectra of 80% acetone pigment extracts with the spectra of the individual pigments [45]. From the total number of Chls and the Chl *a/b* ratio, we estimate the Chl *a* and Chl *b* content. The number of Cars per Lhca is calculated from the Chl/Car ratio of the PSI–LHCI of higher plant (4.8 ( $\pm$  0.1), [25]) assuming 100 Chls and 22 Cars per core, as in cyanobacteria [2]. It follows that in higher plants, the peripheral antenna contains 13.4 Car, corresponding to 3.4 ( $\pm$  0.2) Cars per Lhca. We assume the number of Cars per Lhca to be the same in Lhcas of *C.r.* From the Chls and Car content, we can estimate the fraction of excitation in the core and the peripheral antennas (see Appendix A and Table A.1).

### 2.2. Steady state measurements

Absorption spectra were measured on a Varian Cary 4000UV–Vis spectrophotometer and fluorescence spectra on a Fluorolog spectrofluorimeter (Jobin Yvon Horiba). All spectra were measured at room temperature (RT) and at 77 K (by using a liquid N<sub>2</sub> Horiba FL-1013 LN dewar with a home build cuvette holder) in a plastic cuvette 10 mm  $\times$  3 mm. To avoid self-absorption, samples were diluted to an OD of 0.07 at the Q<sub>y</sub> maximum (1 cm path length) in a buffer containing 10 mM Tricine (pH 7.8) and 0.03% n-Dodecyl- $\alpha$ -D-maltoside ( $\alpha$ -DM). Circular-dichroism (CD) spectra were measured at 10 °C on a Chirascan-Plus CD Spectrometer (Applied Photophysics, Surrey). All presented spectra are scaled to the Chl content: the absorption spectra were integrated between 630 nm and 750 nm and scaled according to the oscillator strength of the particle, by using the estimated number of Chls in the particle (Table 1) and the ratio of 0.7 for the oscillator strength of Chl *b* and Chl *a* in the Q<sub>y</sub> region. The CD spectra were scaled to the integrated area under the absorption between 630 nm and 750 nm (which were scaled to the particles' oscillator strengths as described above).

### 2.3. Time-resolved measurements

The picosecond-time-resolved fluorescence measurement were performed with a Streak Camera setup as described previously ([27, 46]) adapted with a Coherent Vitesse Duo containing an integrated 10 W Verdi CW laser (output wavelength 532 nm) both seeding the Vitesse ultra fast oscillator (output wavelength 800 nm, average power  $\approx$  100 mW, pulse width  $\approx$  100 fs, repetition rate 80 MHz) and pumping the regenerative amplifier Coherent RegA 9000 (output wavelength 800 nm, average power  $\approx$  1 W, pulse width 180–200 fs, tunable repetition rate between 10 kHz and 300 kHz). The output of the RegA fed the optical parametric amplifier Coherent OPA 9400 (output wavelength from 470 nm to 770 nm, average power up to a few mW). The frequency-doubled light (400 nm) in the OPA could also be used as an output. The repetition rate was set to 250 kHz and the OPA set to generate either the 400 nm or the 475 nm excitation wavelength. The light intensity was modulated with neutral density filters, and residual

800 nm light and white light from the OPA were removed with an interference filter. The excitation polarization was set vertical with a Berek polarization compensator (New Focus, model 5540). The light was focused in the sample with a 15 cm focal length lens resulting in a spot diameter of 50  $\mu\text{m}$  in the sample. Fluorescence emission was collected at right angle by two identical achromatic lenses (B. Halle UV-Achromat  $f = 100$  mm) to collimate the light and then focus it on the input slit (100  $\mu\text{m}$ ) of a spectrograph (Chromex 250IS, 50 grooves/mm ruling, blaze wavelength 600 nm, spectral resolution of 2 nm). Scattered excitation light was removed with an optical long-pass filter. A polarizing filter (Spindler & Hoyer, Type 10 K) was placed in between the two achromatic lenses to collect light polarized at magic angle ( $54.7^\circ$ ) with respect to the excitation polarization. After the spectrograph, the light was focused on the input slit (40  $\mu\text{m}$ ) and then on the photo-cathode of the streak camera Hamamatsu C5680 mounted with the M5675 Synchroscan unit (triggered by the Vitesse oscillator) and the Digital CCD Camera Hamamatsu Orca R2 (read out speed 8.5 frame/s). Spectral calibration was done with an Argon lamp (Oriel Instruments Argon lamp model 6030) and spectrotemporal sensitivity (shading) correction [46] with a homogeneous white light source (Xenon lamp, Osram HLX 64642 24 V 150 W GER i 028).

Fluorescence was detected from 590 nm to 860 nm and 0 to 155 ps (time range 1, TR1, temporal response: 4–5 ps) and 0 to 1500 ps (TR4, temporal response: 18 ps). Each dataset consisted of a sequence of images: 10 images of 5 min at TR1 and 15 images of 1 min at TR4. Image sequences were corrected for background, shading and jitter (temporal drift between images within an image sequence) and finally averaged in HPD-TA 8.4.0 (Hamamatsu). These corrected datasets were binned to 2 nm, and zoomed between 640 nm and 800 nm in Glotaran 1.3 [47].

Samples were in 10 mM Tricine (pH 7.8), 0.03%  $\alpha$ -DM, 0.5 M sucrose, and measured in a 10 mm  $\times$  10 mm quartz cuvette at room

temperature (RT). OD at the  $Q_y$  maximum was 0.98 (Full PSI-LHCI) and 0.86 (Small PSI-LHCI). To avoid self-absorption, the laser beam was focused in the sample close to the cuvette wall and emission was collected at right angle close to the entry point of the laser beam into the cuvette. To avoid singlet-singlet annihilation by multiple simultaneous excitation of PSI-LHCI complex, the pulse energy was reduced to 0.6 nJ. To avoid singlet-triplet annihilation, the sample was stirred with a magnet bar. A power study confirms the absence of annihilation (results not shown).

#### 2.4. Data analysis of time-resolved measurements

The streak camera datasets were analyzed globally with a sequential model in order to extract a minimum number of exponential components  $n$  (with increasing lifetimes  $\tau_n$ ) that can satisfactorily describe the data (no structure in the residuals). The two datasets from the same experimental condition (corresponding to the two TRs) were fitted simultaneously with the same kinetic scheme and spectra. The fit yields Evolution Associated Spectra (EAS) characterizing the spectral evolution (e.g. the third EAS rises with the second lifetime and decays with the third lifetime). Decay Associated Spectra (DAS) corresponding to a loss or a gain of emission at specific lifetimes, were calculated from the EAS ([48,49,46]). The raw decay measured at one detection wavelength ( $\lambda$ ) can be written as a sum of exponential decays (convoluted by the IRF) weighted by their DAS ([48,49,46]):  $\text{Decay}(\lambda, t) = \sum_n [\text{DAS}_n(\lambda) \cdot (\text{IRF} \otimes \exp(-t/\tau_n))]$ . The IRF was modeled as the sum of two Gaussians, with full-widths at half maximum (FWHM) of 4–5 ps (94.5% relative integrated area) and 21 ps (5.5%) for TR1 and 18 ps (92.6%) and 288 ps (8.4%) for TR4.

The average decay time  $\tau_{\text{av CS}}$  (Eq. (1)) characterizes the time until CS occurs (for open RCs) and is calculated by considering only the

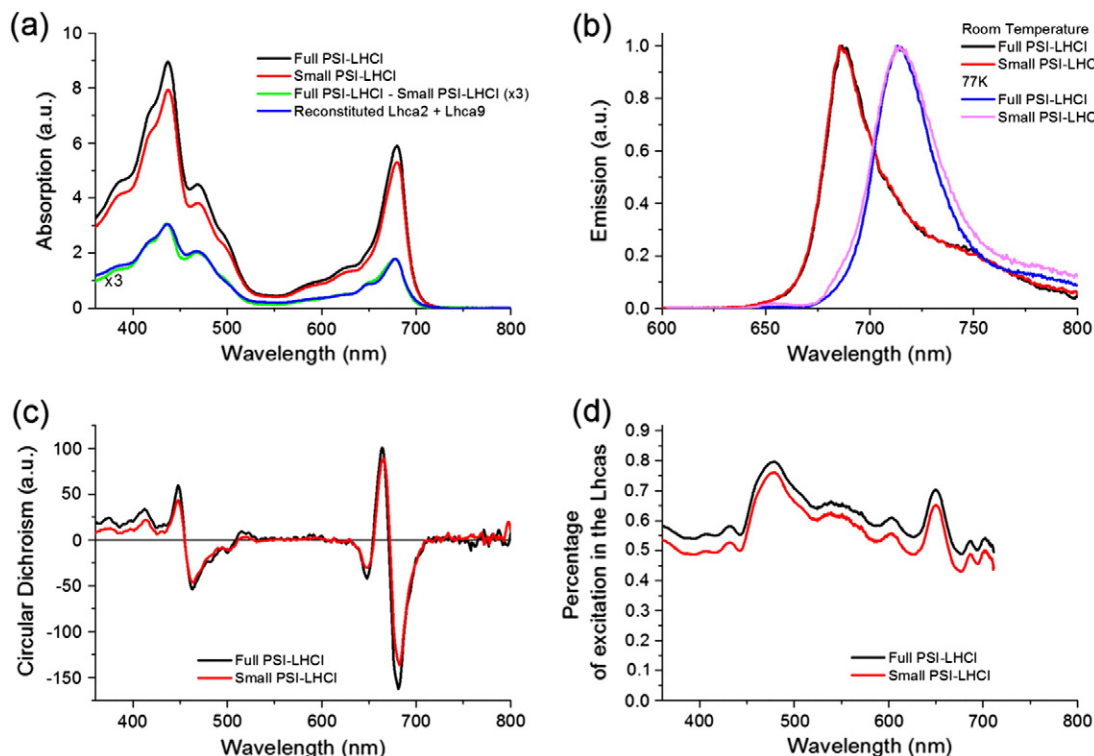


**Fig. 1.** Steady state absorption and emission spectra. (a) RT absorption spectra of Full PSI-LHCI (black) and Small PSI-LHCI (red, scaled to their Chl content, see [Materials and methods](#)) and their difference spectrum (green, enlarged by 3). The difference spectrum overlaps well with the sum of the absorption spectra of reconstituted Lhca2 and Lhca9 (blue, normalized to the  $Q_y$  maximum of the difference spectrum); (b) fluorescence emission (upon 475 nm excitation) of Full PSI-LHCI and Small PSI-LHCI at RT (black and red respectively) and at 77 K (blue and pink respectively), normalized to the maximum; (c) CD at 10 °C of Full PSI-LHCI (black) and Small PSI-LHCI (red) (scaled to the Chl content, see [Materials and methods](#)); (d) Percentage of excitation in the peripheral antenna relative to the entire complex. The absorption of Lhcas is obtained after subtracting the absorption of the core from that of the PSI-LHCI particles (both scaled to the Chl content, see [Appendix A-Method 1](#)).

components attributed to the PSI–LHCI kinetics (excluding components attributed to e.g. disconnected species).

$$\tau_{\text{av CS}} = \frac{\sum_n (\tau_n \cdot A_n)}{\sum_n A_n} \quad 1$$

In Eq. (1),  $A_n$  is the area under the DAS of the  $n$ -th component (i.e. its total amplitude). This approach excludes all components associated with energy transfer in the average decay time calculation, since their positive and negative contributions will cancel (assuming no superradiant or dark states). In cases where transfer components yielded  $A_n < 0$  this was attributed to noise, and  $A_n$  was set to zero.

The data were further analyzed by a target fit ([48–50]) of all eight streak camera datasets simultaneously with the model described in Scheme 1. The model consists of two compartments for Small PSI–LHCI and three for Full PSI–LHCI. The additional compartment in Full PSI–LHCI (green box in Scheme 1) represents the difference between the two PSI particles and can be structurally associated with the two antennas Lhca2 and Lhca9. Species Associated Spectra (SAS), characterizing the emission properties of each species, were estimated by means of a non-negative least-squares variable projection algorithm [51]. Equilibria could be estimated under the assumption of equal oscillator strength of all species (equal area under the SAS, [52]). All rate constants were estimated (uncertainties ranging from 0.8% to 3%) as well as the free-energy difference between the different compartments (uncertainties ranging from 0.2% and 1.3%). Some kinetics faster than the time-resolution were visible around  $t_0$  (Fig. 2). These were modeled as precursors of the other compartments (see Appendix B.1 for more details). Additionally the model contained two functionally disconnected species with small population (between 1.0% and 6.8%) and ns-lifetimes. The full kinetic scheme is presented in Appendix B.1.

### 3. Results

#### 3.1. Steady state characterization

The steady state absorption and fluorescence emission spectra of Full and Small PSI–LHCI are presented in Fig. 1 a and b. The absorption maximum in the  $Q_y$  region at room temperature (RT) is at 679.5 nm for both complexes, as previously observed [15]. The estimated number of Chls in the PSI–LHCI particles (Table 1) was used to scale the absorption spectra to their Chl content (see Materials and methods). The absorption difference spectrum between the two PSI–LHCI particles (Fig. 1a, green) matches the average absorption of reconstituted Lhca2 and Lhca9 (Fig. 1a, blue), indicating that the presence/absence of these two complexes is the main difference between the two preparations.

The maxima of the fluorescence emission spectra at RT and 77 K for both particles were 687 nm and 714.5 nm respectively (Fig. 1b) in agreement with previous results [15].

To check whether the dissociation of Lhca2 and 9 affects the overall organization of PSI–LHCI, circular dichroism (CD) spectra were measured (Fig. 1c). The high similarity between the CD spectra of the two particles indicates that the loss of the two Lhca subunits does not have large secondary effects on the supercomplex organization.

#### 3.2. Time-resolved fluorescence and global sequential analysis

To get insights into the processes of excitation energy transfer and trapping in large systems, it is useful to compare the decay kinetics upon selective excitation of the core and the peripheral antennas ([53, 54]). The difference in absorption between the core and the peripheral antennas is emphasized at 400 nm and 475 nm (Fig. 1d): The largest absorption from the peripheral antenna is visible at 475 nm ( $\approx 80\%$ , see Table A.1) whereas the core and the peripheral antennas have almost the same absorption at 400 nm. Therefore these two

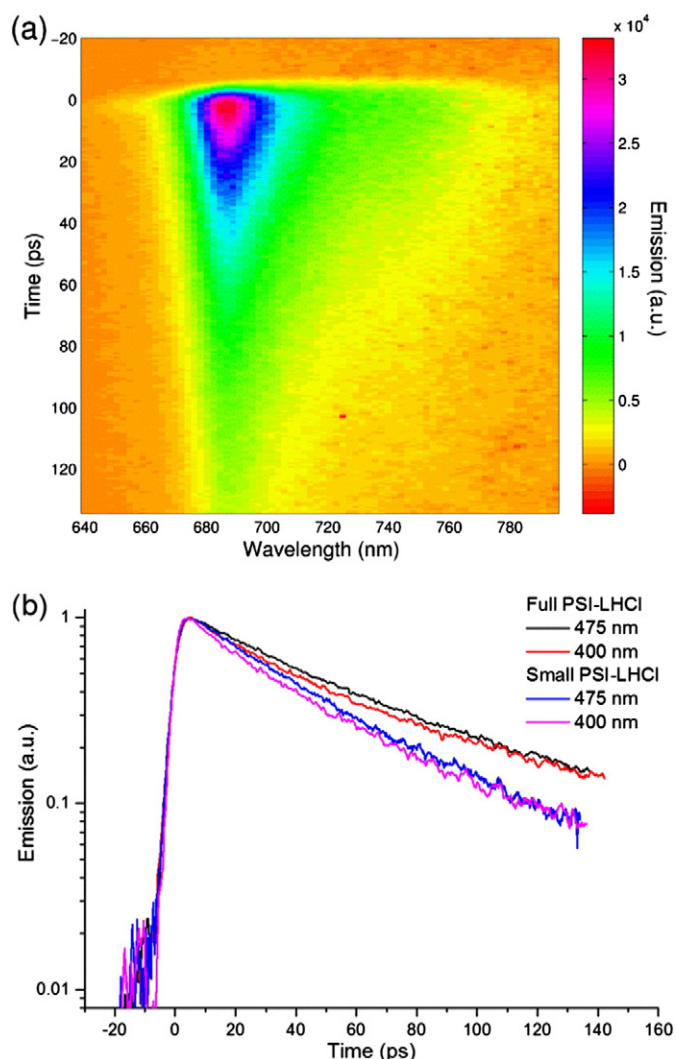


**Fig. 2.** Time resolved fluorescence results. (a) Streak camera image of Full PSI–LHCI upon 475 nm excitation for the short time range. Colors represent the fluorescence emission intensity from zero (orange) to high fluorescence (red); (b) fluorescence decay kinetics (integration from 640 nm to 800 nm) upon 475 nm and 400 nm for Full PSI–LHCI (black and red, respectively) and Small PSI–LHCI (blue and pink, respectively). The decays are normalized to their maximum.

wavelengths were used for excitation when measuring time-resolved fluorescence kinetics with a streak camera setup.

Four parallel experiments were performed: Small and Full PSI–LHCI upon 400 nm and 475 nm excitation. Each sample/excitation combination was measured at two time windows (short time range, 0–155 ps, and long time range, 0–1500 ps), yielding eight streak camera datasets. A typical dataset is presented in Fig. 2a.

When comparing the fluorescence decay integrated over all wavelengths (Fig. 2b) two preliminary observations can be made, which are in line with the expectations: (i) Full PSI–LHCI has a slower overall decay than Small PSI–LHCI at both excitation wavelengths, in agreement with the difference in antenna size and (ii) for both particles the overall decay upon 400 nm excitation is faster than upon 475 nm, in agreement with a preferential excitation of the peripheral antenna at 475 nm.

The sequential analysis showed that at least four exponentially decaying components are required to describe the data. The Decay Associated Spectra (DAS) of Full PSI–LHCI measured upon 400 nm excitation are presented in Fig. 3b (dash lines). The fastest component (1.0 ps) represents excitation energy transfer from blue Chls (a mixture

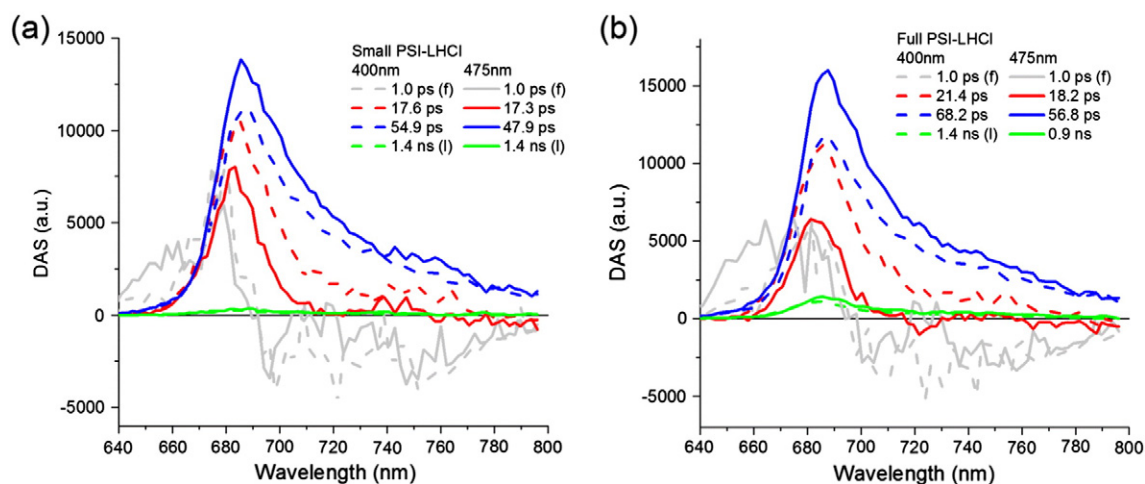
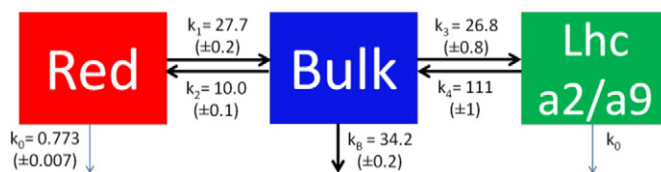


**Fig. 3.** DAS of (a) Small PSI-LHCI and (b) Full PSI-LHCI upon 400 nm (dash lines) or 475 nm (solid lines) at RT. In each experiment, the two different time windows were fitted simultaneously (see **Materials and methods**). Some parameters were fixed (f) and the fourth lifetimes were linked (l) through all experimental conditions (except for Full PSI-LHCI upon 475 nm whose residuals were significantly improved with an independent fit of this lifetime).

of Chls *b* and blue Chls *a*) to red Chls *a*. In particular, Chls *b* emission is visible upon 475 nm excitation at  $\approx 650$  nm detection wavelength (Fig. 2a) and disappears within  $\approx 1$  ps. The weak emission intensity from these Chls *b* prevents accurate estimation of the rate of their depopulation. We therefore fixed it to 1 ps in all the experiments ((f) = fixed in Fig. 3 and Table 2), in line with energy transfers components reported in Lhca complexes ([55,56]).

The second (21.4 ps) and the third component (68.2 ps) represent mainly decay processes. Above 700 nm the second DAS is smaller than the third, indicating that the second component contains less red forms emission. Additionally the expected positive vibrational band is partially missing in the second DAS, meaning that some energy transfer occurs on this time scale. This is more pronounced upon 475 nm excitation than 400 nm, suggesting that it is associated with absorption by Lhcas. The third component represents a pure fluorescence decay and accounts for most of the trapping. The fourth component has a small amplitude (a few percent, see Table 2) and a lifetime of 1.4 ns, which is close to the lifetime of the reconstituted Lhca monomers in plants [57]. The DAS of this ns-component was blue shifted respect to the other DAS. These results suggest that this component is due to a mixture of disconnected Lhcas and Chls that are not part of the PSI-LHCI dynamics.

A similar set of components describes the decay measured in the other experimental conditions (Fig. 3). In all experiments, the first component represents energy transfer from blue Chls to red Chls *a*. For both excitation wavelengths, the second (red) and the third components



**Scheme 1.** Target model for the simultaneous fit of all eight datasets (Full PSI-LHCI and Small PSI-LHCI measured upon 400 nm and 475 nm, with detections windows of 155 ps and 1500 ps). The estimated rate constants ( $\text{ns}^{-1}$ ) are indicated with the fit uncertainties. Full and Small PSI-LHCI have the Red and Bulk compartments in common (identical rate constants, SAS and initial population ratio).

(blue) have shorter lifetimes in Small PSI-LHCI than in Full PSI-LHCI. These lifetimes are shorter upon 475 nm excitation (solid lines) than upon 400 nm excitation (dash lines). This is mainly due to a larger contribution of EET following 475 nm excitation, which indicates that EET in the range of 15–20 ps occurs between the Lhcas or from the Lhcas to the core. A fourth component representing disconnected species was present with low amplitude in all experiments (Table 2).

Upon 400 nm and 475 nm excitation, the average decay time  $\tau_{\text{av CS}}$  increases from 40.3 ps to 41.5 ps for Small PSI-LHCI and from 49.7 ps to 51.4 ps for Full PSI-LHCI (Table 2). The presence of Lhca2 and Lhca9 in Full PSI-LHCI increases the average decay time by 9.4 ps at 400 nm and by 9.9 ps at 475 nm compared to Small PSI-LHCI.

### 3.3. Target analysis

To understand the EET and trapping processes in more detail, a target analysis was used to fit all datasets simultaneously. This enables estimation of rate constants, and free energy differences, between different compartments within a chosen kinetic model.

The target model (Scheme 1) consists of two compartments (Red and Bulk) for both particles, and an additional compartment for Full PSI-LHCI, representing the ensemble of Lhca2 and Lhca9 (Lhca2/a9).

**Table 3**  
Estimated relative initial populations (error  $\pm 0.5\%$ ) of the compartments of the target model (Scheme 1). The energy input ratio of the Red and Bulk compartments is linked between the two samples when measured upon the same wavelength.

	Red	Bulk	Lhca2/a9
Small PSI-LHCI upon 400 nm	8.8%	91.2%	n.a.
Small PSI-LHCI upon 475 nm	11.5%	88.5%	n.a.
Full PSI-LHCI upon 400 nm	8.0%	82.7%	9.3%
Full PSI-LHCI upon 475 nm	10.4%	79.9%	9.7%

**Table 2**

Lifetimes obtained from the sequential analysis of the fluorescence decays of the two PSI-LHCI particles measured upon 400 nm and 475 nm excitation with their relative amplitude (i.e.  $A_n / \sum A_n$ , see **Materials and methods**) and average decay time  $\tau_{\text{av CS}}$  (the ns component is not considered in the calculation, see details and Eq. (1) in **Materials and methods**). The contributions were set to 0% in case the area under the DAS was negative (see **Materials and methods**). Some lifetimes were fixed (f) or linked (l).

	Small PSI-LHCI		Full PSI-LHCI	
	400 nm	475 nm	400 nm	475 nm
$\tau_1$ (ps)	1.0 (f)			
Relative amplitude	0%			
$\tau_2$ (ps)	17.6	17.3	21.4	18.2
Relative amplitude	38.5%	20.4%	37.7%	12.3%
$\tau_3$ (ps)	54.9	47.9	68.2	56.8
Relative amplitude	60.0%	77.1%	57.5%	75.7%
$\tau_4$ (ns)	1.4 (l)			0.9
Relative amplitude	1.5%	2.0%	4.8%	6.4%
Average decay time $\tau_{\text{av CS}}$ (ps)	40.3	41.5	49.7	51.4

On a picosecond time scale the compartments are populated from precursors, with relative amounts according to Table 3 (see Appendix B.1 for details). The compartments have the same natural decay rate constant  $k_0$ , except for Bulk where the charge separation occurs in the RC (trapping with specific rate constant  $k_B$ ). Energy is transferred between Red and Bulk, and between Bulk and Lhca2/a9.

The Species Associated Spectra (SAS) estimated from the target analysis for all the datasets, are shown in Fig. 4. The Bulk SAS (blue) corresponds to bulk Chl *a* emission. The Red SAS is red-shifted compared to the Bulk SAS and represents red Chls and a few normal Chls in fast equilibrium with them. The Lhca2/a9 SAS (green) shows a more red-shifted spectrum compared to Bulk but clearly less than Red.

Two additional compartments account for the very low population of disconnected species, either disconnected Lhcas or disconnected Chls (see Appendix B.1 for details).

The relative initial populations of the compartments of Scheme 1 are given in Table 3.

The Chl *a/b* ratio differs between compartments, as follows from the relative initial populations at the two excitation wavelengths (Table 3). Bulk is more core-like with the input decreasing upon 475 nm compared to 400 nm excitation (less Chl *b*), whereas Red and Lhca2/a9 are more Lhca-like with the input increasing upon 475 nm compared to 400 nm excitation (more Chl *b*). Bulk receives more than  $\approx 80\%$  of the excitations, which indicates that it contains Chls from the peripheral antenna in addition to those of the core.

The equilibration between Bulk and Lhca2/a9 is four times faster than the equilibration between Red and Bulk ( $(k_1 + k_2)^{-1} \approx 4 \times (k_3 + k_4)^{-1}$ , see Scheme 1). This is explained by the further red-shifted SAS of Red compared to the Lhca2/a9 SAS which leads to a smaller spectral overlap and thus a slower back transfer to the Bulk compartment.

The differences in free energy  $\Delta G$ , enthalpy  $\Delta H$  and entropy  $\Delta S$  between the compartments enable estimation of the number of Chls in each of them (see Appendix B.2 for details). From the forward and backward rate constants in Scheme 1, we calculate that the free energy of Red and Lhca2/a9 is respectively 26 and 36 meV higher than Bulk. The enthalpy, approximated as the average spectral position of the SAS yields  $13,930 \pm 50 \text{ cm}^{-1}$  ( $1727 \pm 6 \text{ meV}$ ) for Red,  $14,255 \pm 10 \text{ cm}^{-1}$  ( $1767 \pm 2 \text{ meV}$ ) for Bulk and  $14,076 \pm 20 \text{ cm}^{-1}$  ( $1745 \pm 3 \text{ meV}$ ) for Lhca2/a9. So the enthalpies of Red and Lhca2/a9 are respectively  $40 \pm 5$  and  $22 \pm 5 \text{ meV}$  lower than Bulk. The entropy difference (multiplied by the temperature  $T = 293 \text{ K}$ ) of Red and Lhca2/a9 with Bulk corresponds to  $66 \pm 5$  and  $58 \pm 2 \text{ meV}$  respectively. This gives a Chls *a* ratio of  $0.07 \pm 0.02$  between Red and Bulk and of  $0.100 \pm 0.005$  between Lhca2/a9 and Bulk (see Appendix B.2). Combining this with the estimated total number of Chls *a* (Table 1), it

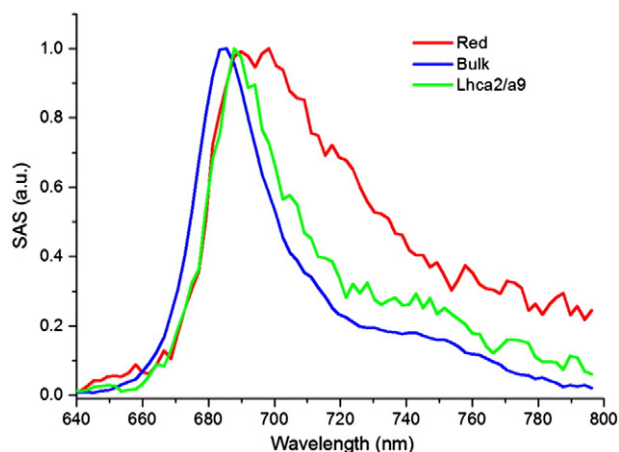


Fig. 4. SAS estimated for all four experimental conditions (eighth datasets) simultaneously fitted with the kinetics model of Scheme 1. The SAS are normalized to their maximum.

Table 4  
Amplitude matrices in the case of Small PSI-LHCI and Full PSI-LHCI upon 400 nm.

	Small PSI-LHCI		Full PSI-LHCI			
	Red	Bulk	Red	Bulk	Lhca2/a9	
18.3 ps	-0.227	0.599	6.6 ps	-0.016	0.199	-0.139
55.8 ps	0.306	0.322	22.6 ps	-0.196	0.312	0.124
			60.4 ps	0.283	0.337	0.094

follows that Red contains  $12 \pm 2$  Chls *a*, Bulk  $163 \pm 3$  and Lhca2/a9  $16 \pm 1$ .

The temporal concentration profiles of each compartment in the target model are described by the amplitude matrices (see Appendix B.3 for details). The amplitude matrices for measurements upon 400 nm excitation are presented in Table 4 (see Table B.3.1 for measurements upon 475 nm).

The 6.6 ps component is only present in Full PSI-LHCI and mainly represents the energy transfer from Bulk to Lhca2/a9. In both particles, the  $\approx 20$  ps component shows ingrowths of Red and trapping from Bulk. During the last component, the population of all the compartments decreases because of the trapping from Bulk. Similar observations can be made for the kinetics upon 475 nm excitation (Table B.3.1). The two trapping times are slowed down in the presence of Lhca2 and Lhca9 antennas: from 18.3 ps to 22.6 ps for the first component of the trapping and from 55.8 ps to 60.4 ps for the second one.

#### 4. Discussion

The average decay time of the PSI-LHCI complex of *C.r.* containing nine Lhcas per core complex (Full PSI-LHCI) is 49.7 ps upon 400 nm and 51.4 ps upon 475 nm, very close to those of higher plant PSI-LHCI (48 ps upon 440 nm excitation and 53 ps upon 475 nm excitation for *A.t.* [37]). This strongly suggests that the antenna enlargement in *C.r.* PSI-LHCI compared to PSI-LHCI of higher plant is compensated by the presence of red forms with higher energy than in higher plants, resulting in a similar average decay time of PSI-LHCI in the two organisms.

Excitation dynamics of isolated Full PSI-LHCI of *C.r.* were measured previously by several groups, with reported average decay times varying from 24 ps to 59 ps ([40,39,35,41]). The shorter lifetimes might have arisen from differences in protein composition, especially considering that instability of the large PSI-LHCI complex that easily loses part of the antenna [15]. Indeed, Giera et al. (2014) [41] studied a PSI-LHCI preparation with a small antenna size (Chl *a/b* 7.5 vs. 4.4 of our PSI-LHCI complex) observing an average decay time of 24.3 ps, a

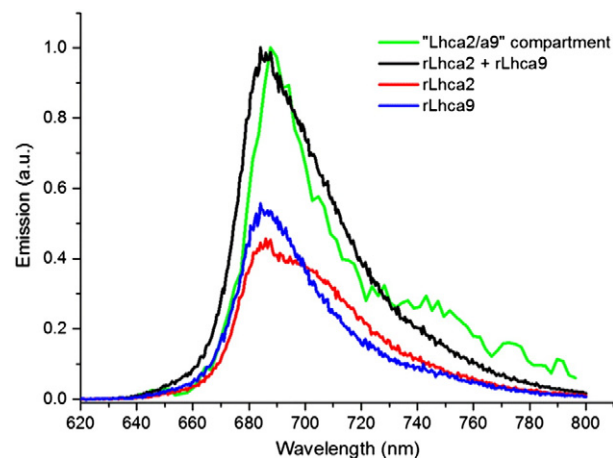


Fig. 5. Comparison of the Lhca2/a9 SAS (green) and the RT steady state fluorescence of the two reconstituted antennas Lhca2 and Lhca9 [14] and their sum (red, blue and black respectively). Steady state spectra were normalized to equal area, and the SAS was scaled so the peak value equals that of the sum of steady state spectra.

value close to that of the core complex [37]. The longer lifetimes in ([39, 35]) are probably due to some photosystem II impurity present in the preparations as indicated by the authors [58]. These impurities are absent in our preparation [15] thanks to the presence of a His tag on PsaA [59] which facilitates the purification.

A more detailed insight in EET and trapping in the complexes is obtained from target analysis. Most of the Chls associated with PSI are present in the Bulk compartment. This compartment contains 163 Bulk Chls, including the RC, and shows a trapping rate  $k_B$  of  $(29.2 \text{ ps})^{-1}$ .  $k_B$  was estimated at  $(18.9 \text{ ps})^{-1}$  in higher plants [37]. The difference is well explained by the larger amount of Chls in Bulk relative to the “Core Bulk” compartment used in the target model for higher plants ( $\approx 100$  Chls *a*): the average population of *C.r.* RC is  $\approx 1.63$  times lower than in higher plants, which (in a simple trapping limited approach, [60]) leads to a  $\approx 1.63$  times slower trapping from Bulk as observed here. The good similarity between higher plants and *C.r.* indicates that the Bulk Chls are equally well-connected in the two species, including the 63 Bulk Chls *a* associated with the peripheral antenna.

The Red compartment contains 12 Chls *a* including the red-most forms. Two trapping components of 18.3 and 55.8 ps are resolved because of the ingrowth process occurring in Red (directly from the precursors or from Bulk after energy transfer). The trapping is slowed down relative to the hypothetical particle composed of only Bulk. Red is preferentially excited at 475 nm, indicating that (part of) the red-most forms are located in or close to the peripheral antenna, with Lhca4 being the best candidate as indicated by the analysis of reconstituted complexes [14].

The simultaneous target analysis of the samples with and without Lhca2 and Lhca9 enabled us to quantitatively describe the role of these Lhcas in the EET and trapping kinetics of PSI–LHCI. The estimated number of Chls *a* in the Lhca2/a9 compartment (16) is consistent with the estimated difference in Chls *a* between Full and Small PSI–LHCI (18, see Table 1). The Lhca2/a9 SAS agrees well with the sum of the emission spectra of Lhca2 and Lhca9 (Fig. 5) thus confirming that these complexes have a red-shifted spectrum compared to the Bulk Chls (Fig. 4) but they do not contain the most-red forms (which are present in the Red compartment). In the analysis, the presence of Lhca2/a9 results in an additional energy transfer step with a 6.6 ps lifetime and a slowdown of the two main trapping components by 4.3 ps for the first one and by 4.6 ps for the second one.

From the average decay time  $\tau_{av \text{ CS}}$ , the trapping efficiency, i.e. the quantum yield of CS ( $\Phi_{CS}$ ), can be calculated using  $\Phi_{CS} = 1 - \tau_{av \text{ CS}} / \tau_{no \text{ CS}}$  [60], where  $\tau_{no \text{ CS}}$  is the average decay time in the (hypothetical) case that CS cannot occur.  $\tau_{no \text{ CS}}$  is approximated as the average decay time of plant Lhca monomer ( $\sim 2$  ns, [57]), the closest system of PSI–LHCI where CS does not occur. In Photosystem II, it was shown that  $\Phi_{CS}$  decreases with increasing antenna size [61]. Nevertheless, this loss in efficiency is compensated by a larger absorption cross section that enhances the absorption capacity enough to increase the product of the number of Chls *a* in PSII times the quantum yield  $\Phi_{CS}$ . For PSI–LHCI the calculations show that even with an increasing average decay time, the trapping efficiency remains very high (Table 5).

The increased absorption cross-section of Full PSI–LHCI of *C.r.* enables it to harvest  $\approx 41\%$  more photons than PSI–LHCI of *A.t.* (area

under their scaled absorption spectra), without affecting trapping efficiencies. This is very advantageous in low light environments. Full PSI–LHCI is slower than Small PSI–LHCI in *C.r.* but their trapping efficiency are comparable: the red forms contained in Lhca2 and Lhca9 slow down the average decay time but have almost no effect on the trapping efficiency.

## Acknowledgments

This work was supported by the ERC consolidator grant 281341 (ASAP) to RC and by the Netherlands Organization for Scientific Research (NWO) through a Vici grant to RC and a Veni grant to BvO. We acknowledge Jos Thieme for technical support with the initial streak camera experiments.

## Appendix A. Fraction of excitation in the core and the peripheral antennas

Fractions of excitation in either the core or the peripheral antennas were calculated (see Method 1 and Method 2 below, and the results in Table A.1) to choose the excitation wavelengths where the fraction differences were the largest.

Method 1: The absorption spectrum of the peripheral antenna ( $A_{LHCI}$ , including gap Chls) is obtained from the difference absorption spectrum PSI–LHCI ( $A_{PSI-LHCI}$ , from *C.r.*, this study) minus core ( $A_{core}$ , from *A.t.* [37]):  $A_{LHCI} = A_{PSI-LHCI} - A_{core}$  (Fig. A.1).  $A_{PSI-LHCI}$  and  $A_{core}$  were scaled to their Chl content (see Materials and methods). PSI core absorption from *A.t.* was used in this study because no conclusive biochemical isolation of *C.r.* PSI core has been done so far (presence of disconnected antenna oligomers in the PSI core preparation visible in time-resolved data [39,35,62,63, 56]). The percentage of photons absorbed in the peripheral antenna was calculated as  $A_{LHCI} / A_{PSI-LHCI}$  (Fig. 1d of the main text).

Method 2: The extinction coefficients of the different pigments were assumed equal to those of pigments extracted in 80% acetone (considering the absorption in acetone to be 15 nm blue-shifted compared to the absorption in proteic environment) and were multiplied by the estimated number of each pigment (Table 1 of the main text). The energy transfer from Cars to Chls occurs faster than our time resolution and is assumed to be 70% efficient as observed in Lhcas of higher plants [37] and in the PSI core of cyanobacteria [64].

## Appendix B. Target analysis

### B.1. Kinetic scheme

The complete kinetic model used for the target analysis is presented in Scheme B.1.1.

All datasets were fitted with the same set of rate constants and SAS (except for one rate, see below). The only difference between the data obtained from the two excitation wavelengths was the relative population of the Red, Bulk and Lhca2/a9 compartments from the Precursors

**Table 5**

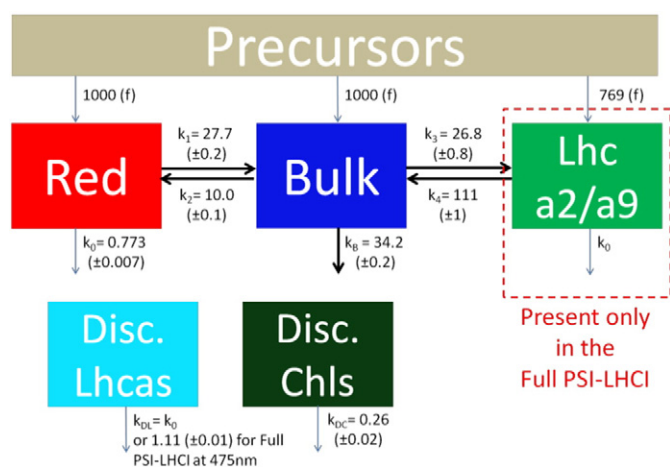
Comparison of average decay times and trapping efficiency between *A.t.* and the two *C.r.* PSI–LHCI.

	<i>A.t.</i> PSI–LHCI	<i>C.r.</i> Full PSI–LHCI	<i>C.r.</i> Small PSI–LHCI
Average decay time (ps)	48 ps–53 ps	51.4 ps	41.5 ps
$\tau_{av \text{ CS}} = \sum A_i \times \tau_i$	[37]		
Trapping efficiency	97.3%–97.6%	97.4%	97.9%
$\Phi_{CS} = 1 - \tau_{av \text{ CS}} / \tau_{no \text{ CS}}$			

**Table A.1**

Initial distribution of excitations over core and peripheral antennas pigments (Chls and Cars) calculated with two methods (Method 1/Method 2) to estimate the uncertainties.

	Small PSI–LHCI		Full PSI–LHCI	
	400 nm	475 nm	400 nm	475 nm
Excitation wavelength	400 nm	475 nm	400 nm	475 nm
Percentage of excitation in the core antenna pigments	51%/53%	24%/23%	45%/47%	21%/19%
Percentage of excitation in the peripheral antenna pigments	49%/47%	76%/78%	55%/53%	79%/81%



**Scheme B.1.1.** Complete kinetic model including precursors and compartments associated with the disconnected species. Rates are indicated in  $\text{ns}^{-1}$ , with fit uncertainties.

compartment (Table 3 of the main text). The precursor compartment contains emission from pigments that transfer energy among themselves faster than the time resolution of our instrument ( $\approx 2$  ps). Its spectrum contains Chl *a* and Chl *b* (especially visible after 475 nm excitation). It rapidly (1–1.3 ps) depopulates into Red, Bulk and Lhc a2/a9.

The simultaneous target analysis of all datasets enabled the differentiation of the disconnected species into two compartments. The disconnected species are either disconnected Lhcas (named “Disc. Lhcas”) whose rate constant  $k_{DL}$  is  $(1.29 \text{ ns})^{-1}$ , or disconnected Chls (named “Disc. Chls.”) whose rate constant  $k_{DC}$  is  $(3.8 \text{ ns})^{-1}$ . The Disc. Lhcas SAS (cyan in Fig. B.1.1) is indeed Lhca-like as indicated by its higher red emission compared to the Bulk SAS (blue). The Disc. Chls SAS (dark green in Fig. B.1.1) has the typical blue-shifted spectrum of free Chls with the expected emission maximum around 675 nm.

The decay rates of Disc. Lhcas were linked for all experimental conditions except for Full PSI-LHCI upon 475 nm whose lifetime was fitted independently to improve significantly the residuals at long time scale. The other fit parameters were not affecting by “unlinking” this decay rate. This difference in decay rates for Disc. Lhcas between the two excitation wavelengths may suggest subpopulations of Lhcas present in the membrane. Further quenched Lhcas could be preferentially excited upon 475 nm.

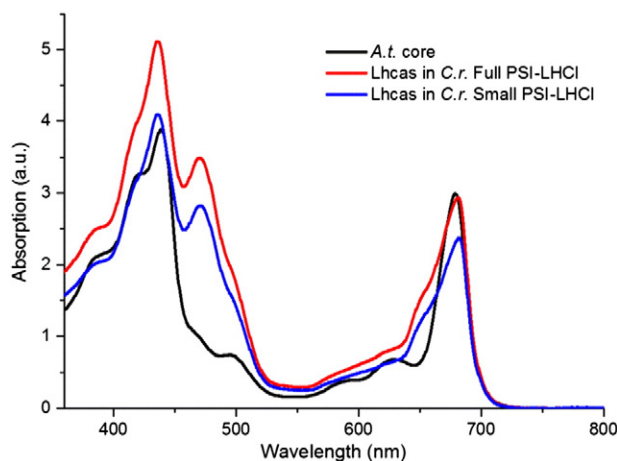
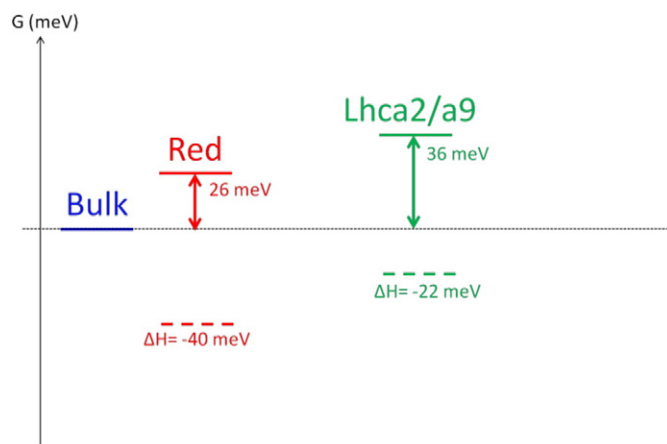


**Fig. A.1.** RT absorption spectra of the core complex from *A.t.* (black) and the peripheral antenna (calculated as in Method 1 below) of *C.r.* in Full PSI-LHCI (red) and Small PSI-LHCI (blue), scaled to their Chl content.



**Scheme B.2.1.** Free energy  $\Delta G$ , enthalpy  $\Delta H$  differences between the compartments and bulk.

### B.2. The differences in free energy $\Delta G$ , enthalpy $\Delta H$ and entropy $\Delta S$

The free energy difference  $\Delta G$  between the compartments and Bulk are presented in Scheme B.2.1. From the forward and backward rate constants,  $\Delta G$  is calculated as  $\Delta G_{ij} = G_j - G_i = -k_B T \ln(k_{i \rightarrow j} / k_{j \rightarrow i})$ . The enthalpy *H* corresponds to the energy level of the Chls contained in one compartment and is approximated in this study as the average spectral position of the SAS.  $\Delta H$  between the compartments and Bulk is represented with dashed lines in Scheme B.2.1.

The entropy difference, calculated from the two previous energy differences with  $T\Delta S = \Delta H - \Delta G$ , represents the thermal activation that enables up-hill EET from the red forms. The ratio of the number of Chls *a* between compartments is obtained with  $\frac{N_i}{N_j} = \exp\left(-\frac{\Delta S_{ij}}{k_B}\right)$ , assuming all excitations on Chl *a* and none on Chl *b*. Knowing the total number of Chls, we can estimate the number of Chls in each compartment (see main text).

### B.3. Amplitude matrices at 475 nm

In amplitude matrices, each compartment populates (negative amplitudes) and depopulates (positive amplitudes) at indicated

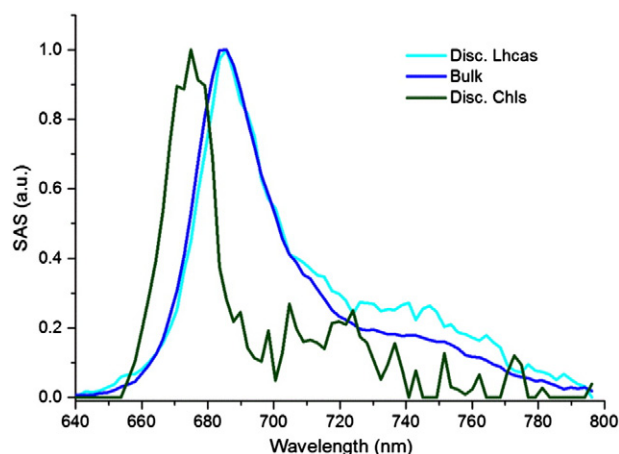


**Fig. B.1.1.** SAS of the disconnected species compared to Bulk (normalized to their maximum).

**Table B.3.1**

Amplitude matrices in the case of Small PSI–LHCI and Full PSI–LHCI upon 475 nm.

Small PSI–LHCI		Full PSI–LHCI				
	Red	Bulk	Red	Bulk	Lhca2/a9	
			6.6 ps	–0.015	0.188	–0.130
18.3 ps	–0.212	0.560	22.6 ps	–0.181	0.288	0.114
55.8 ps	0.318	0.335	60.4 ps	0.292	0.348	0.097

lifetimes (inverse rates). The amplitude matrices for measurements with 400 nm excitation are presented in the main text (Table 4) and with 475 nm in Table B.3.1.

## Transparency document

The Transparency document associated with this article can be found, in online version.

## References

- R. Croce, H. van Amerongen, Natural strategies for photosynthetic light harvesting, *Nat. Chem. Biol.* 10 (2014) 492–501.
- P. Jordan, P. Fromme, H.T. Witt, O. Klukas, W. Saenger, N. Krauß, Three-dimensional structure of cyanobacterial photosystem I at 2.5 Å resolution, *Nature* 411 (2001) 909–917.
- R. Croce, H. van Amerongen, Light-harvesting in photosystem I, *Photosynth. Res.* 116 (2013) 153–166.
- A. Busch, M. Hippler, The structure and function of eukaryotic photosystem I, *Biochim. Biophys. Acta* 1807 (2011) 864–877.
- N. Nelson, Evolution of photosystem I and the control of global enthalpy in an oxidizing world, *Photosynth. Res.* 116 (2013) 145–151.
- Y. Mazor, D. Nataf, H. Toporik, N. Nelson, Crystal structures of virus-like photosystem I complexes from the mesophilic cyanobacterium *Synechocystis* PCC 6803, *eLife* 3 (2014) e01496.
- A. Ben-Shem, F. Frolow, N. Nelson, Crystal structure of plant photosystem I, *Nature* 426 (2003) 630–635.
- A. Amunts, H. Toporik, A. Borovikova, N. Nelson, Structure determination and improved model of plant photosystem I, *J. Biol. Chem.* 285 (2010) 3478–3486.
- H.V. Scheller, P.E. Jensen, A. Haldrup, C. Lunde, J. Knoetzel, Role of subunits in eukaryotic Photosystem I, *Biochim. Biophys. Acta* 1507 (2001) 41–60.
- J.F. Allen, W.B. de Paula, S. Puthiyaveetil, J. Nield, A structural phylogenetic map for chloroplast photosynthesis, *Trends Plant Sci.* 16 (2011) 645–655.
- U. Ganeteg, F. Klimmek, S. Jansson, Lhca5—an LHC-type protein associated with photosystem I, *Plant Mol. Biol.* 54 (2004) 641–651.
- S.S. Merchant, S.E. Prochnik, O. Vallon, E.H. Harris, S.J. Karpowicz, G.B. Witman, A. Terry, A. Salamov, L.K. Fritz-Laylin, L. Marechal-Drouard, W.F. Marshall, L.H. Qu, D.R. Nelson, A.A. Sanderfoot, M.H. Spalding, V.V. Kapitonov, Q. Ren, P. Ferris, E. Lindquist, H. Shapiro, S.M. Lucas, J. Grimwood, J. Schmutz, P. Cardol, H. Cerutti, G. Chanfreau, C.L. Chen, V. Cognat, M.T. Croft, R. Dent, S. Dutcher, E. Fernandez, H. Fukuzawa, D. Gonzalez-Ballester, D. Gonzalez-Halphen, A. Hallmann, M. Hanikenne, M. Hippler, W. Inwood, K. Jabbari, M. Kalanon, R. Kuras, P.A. Lefebvre, S.D. Lemaire, A.V. Lobanov, M. Lohr, A. Manuell, I. Meier, L. Mets, M. Mittag, T. Mittelmeier, J.V. Moroney, J. Moseley, C. Napoli, A.M. Nedelcu, K. Niyogi, S.V. Novoselov, I.T. Paulsen, G. Pazour, S. Purton, J.P. Ral, D.M. Riano-Pachon, W. Riekhof, L. Rymarquis, M. Schroda, D. Stern, J. Umen, R. Willows, N. Wilson, S.L. Zimmer, J. Allmer, J. Balk, K. Bisova, C.J. Chen, M. Elias, K. Gendler, C. Hauser, M.R. Lamb, H. Ledford, J.C. Long, J. Minagawa, M.D. Page, J. Pan, W. Pootakham, S. Roje, A. Rose, E. Stahlberg, A.M. Terauchi, P. Yang, S. Ball, C. Bowler, C.L. Dieckmann, V.N. Gladyshev, P. Green, R. Jorgensen, S. Mayfield, B. Mueller-Roeber, S. Rajamani, R.T. Sayre, P. Brokstein, I. Dubchak, D. Goodstein, L. Hornick, Y.W. Huang, J. Jhaveri, Y. Luo, D. Martinez, W.C. Ngau, B. Otiilar, A. Poliakov, A. Porter, L. Szajkowski, G. Werner, K. Zhou, I.V. Grigoriev, D.S. Rokhsar, A.R. Grossman, The *Chlamydomonas* genome reveals the evolution of key animal and plant functions, *Science* 318 (2007) 245–250.
- D. Elrad, A. Grossman, A genome’s-eye view of the light-harvesting polypeptides of *Chlamydomonas reinhardtii*, *Curr. Genet.* 45 (2004) 61–75.
- M. Mozzo, M. Mantelli, F. Passarini, S. Caffarri, R. Croce, R. Bassi, Functional analysis of Photosystem I light-harvesting complexes (Lhca) gene products of *Chlamydomonas reinhardtii*, *Biochim. Biophys. Acta* 1797 (2010) 212–221.
- B. Drop, M. Webber-Birungi, F. Fusetti, R. Kouril, K.E. Redding, E.J. Boekema, R. Croce, Photosystem I of *Chlamydomonas reinhardtii* contains nine light-harvesting complexes (Lhca) located on one side of the core, *J. Biol. Chem.* 286 (2011) 44878–44887.
- E.J. Boekema, P.E. Jensen, E. Schlodder, J.F. van Breemen, H. van Roon, H.V. Scheller, J.P. Dekker, Green plant photosystem I binds light-harvesting complex I on one side of the complex, *Biochemistry* 40 (2001) 1029–1036.
- B. Gobets, R. van Grondelle, Energy transfer and trapping in photosystem I, *Biochim. Biophys. Acta* 1507 (2001) 80–99.
- R.C. Jennings, G. Zucchelli, E. Engelmann, F.M. Garlaschi, The long-wavelength chlorophyll states of plant LHCI at room temperature: a comparison with PSI–LHCI, *Biophys. J.* 87 (2004) 488–497.
- J.A. Ihalainen, M. Rätsep, P.E. Jensen, H.V. Scheller, R. Croce, R. Bassi, J.E. Korppi-Tommola, A. Freiberg, Red spectral forms of chlorophylls in green plant PSI—a site-selective and high-pressure spectroscopy study, *J. Phys. Chem. B* 107 (2003) 9086–9093.
- R. Croce, A. Chojnicka, T. Morosinotto, J.A. Ihalainen, F. van Mourik, J.P. Dekker, R. Bassi, R. van Grondelle, The low-energy forms of photosystem I light-harvesting complexes: spectroscopic properties and pigment-pigment interaction characteristics, *Biophys. J.* 93 (2007) 2418–2428.
- J. Burke, K. Steinback, I. Ohad, C. Arntzen, Control of photosynthetic competence in the Y-1 mutant of *Chlamydomonas reinhardtii*, *Chloroplast Development*, Elsevier, Amsterdam, 1978, 413–418.
- J.M. Gershoni, I. Ohad, The use of an internal standard for semiquantitative analysis of low temperature (77°K) fluorescence of photosynthetic cells, *Anal. Biochem.* 104 (1980) 315–320.
- F.-A. Wollman, P. Bennoun, A new chlorophyll-protein complex related to Photosystem I in *Chlamydomonas reinhardtii*, *Biochim. Biophys. Acta* 680 (1982) 352–360.
- J. Garnier, J. Maroc, D. Guyon, Low-temperature fluorescence emission spectra and chlorophyll-protein complexes in mutants of *Chlamydomonas reinhardtii*: evidence for a new chlorophyll-a-protein complex related to Photosystem I, *Biochim. Biophys. Acta* 851 (1986) 395–406.
- E. Wientjes, G.T. Oostergetel, S. Jansson, E.J. Boekema, R. Croce, The role of Lhca complexes in the supramolecular organization of higher plant photosystem I, *J. Biol. Chem.* 284 (2009) 7803–7810.
- N.V. Karapetyan, E. Schlodder, R. van Grondelle, J.P. Dekker, The long wavelength chlorophylls of photosystem I, *Photosystem I: The Light-Driven Plastocyanin:ferredoxin Oxidoreductase*, Springer, 2006, 177–192.
- B. Gobets, I.H.M. van Stokkum, M. Rögner, J. Kruij, E. Schlodder, N.V. Karapetyan, J.P. Dekker, R. van Grondelle, Time-resolved fluorescence emission measurements of photosystem I particles of various cyanobacteria: a unified compartmental model, *Biophys. J.* 81 (2001) 407–424.
- T. Morosinotto, J. Breton, R. Bassi, R. Croce, The nature of a chlorophyll ligand in Lhca proteins determines the far red fluorescence emission typical of photosystem I, *J. Biol. Chem.* 278 (2003) 49223–49229.
- T. Morosinotto, M. Mozzo, R. Bassi, R. Croce, Pigment-pigment interactions in Lhca4 antenna complex of higher plants photosystem I, *J. Biol. Chem.* 280 (2005) 20612–20619.
- R. Croce, G. Zucchelli, F.M. Garlaschi, R.C. Jennings, A thermal broadening study of the antenna chlorophylls in PSI-200, LHCI, and PSI core, *Biochemistry* 37 (1998) 17355–17360.
- P. Tapie, Y. Choquet, J. Breton, P. Deleplaire, F.-A. Wollman, Orientation of photosystem-I pigments. Investigation by low-temperature linear dichroism and polarized fluorescence emission, *Biochim. Biophys. Acta* 767 (1984) 57–69.
- R. Bassi, S.Y. Soen, G. Frank, H. Zuber, J.D. Rochaix, Characterization of chlorophyll a/b proteins of photosystem I from *Chlamydomonas reinhardtii*, *J. Biol. Chem.* 267 (1992) 25714–25721.
- Y. Takahashi, T.A. Yasui, E.J. Stauber, M. Hippler, Comparison of the subunit compositions of the PSI–LHCI supercomplex and the LHCI in the green alga *Chlamydomonas reinhardtii*, *Biochemistry* 43 (2004) 7816–7823.
- K. Gibasiewicz, A. Szrajner, J.A. Ihalainen, M. Germano, J.P. Dekker, R. van Grondelle, Characterization of low-energy chlorophylls in the PSI–LHCI supercomplex from *Chlamydomonas reinhardtii*. A site-selective fluorescence study, *J. Phys. Chem. B* 109 (2005) 21180–21186.
- A.N. Melkozernov, J. Kargul, S. Lin, J. Barber, R.E. Blankenship, Spectral and kinetic analysis of the energy coupling in the PS I–LHC I supercomplex from the green alga *Chlamydomonas reinhardtii* at 77 K, *Photosynth. Res.* 86 (2005) 203–215.
- R.C. Jennings, G. Zucchelli, R. Croce, F.M. Garlaschi, The photochemical trapping rate from red spectral states in PSI–LHCI is determined by thermal activation of energy transfer to bulk chlorophylls, *Biochim. Biophys. Acta* 1557 (2003) 91–98.
- E. Wientjes, I.H.M. van Stokkum, H. van Amerongen, R. Croce, The role of the individual Lhcas in photosystem I excitation energy trapping, *Biophys. J.* 101 (2011) 745–754.
- C. Slavov, M. Ballottari, T. Morosinotto, R. Bassi, A.R. Holzwarth, Trap-limited charge separation kinetics in higher plant photosystem I complexes, *Biophys. J.* 94 (2008) 3601–3612.
- A.N. Melkozernov, J. Kargul, S. Lin, J. Barber, R.E. Blankenship, Energy coupling in the PSI–LHCI supercomplex from the green alga *Chlamydomonas reinhardtii*, *J. Phys. Chem. B* 108 (2004) 10547–10555.
- J.A. Ihalainen, I.H.M. van Stokkum, K. Gibasiewicz, M. Germano, R. van Grondelle, J.P. Dekker, Kinetics of excitation trapping in intact Photosystem I of *Chlamydomonas reinhardtii* and *Arabidopsis thaliana*, *Biochim. Biophys. Acta* 1706 (2005) 267–275.
- W. Giera, S. Szweczyk, M.D. McConnell, J. Snellenburg, K.E. Redding, R. van Grondelle, K. Gibasiewicz, Excitation dynamics in Photosystem I from *Chlamydomonas reinhardtii*. Comparative studies of isolated complexes and whole cells, *Biochim. Biophys. Acta* 1837 (2014) 1756–1768.
- E. Wientjes, R. Croce, PMS: photosystem I electron donor or fluorescence quencher, *Photosynth. Res.* 111 (2012) 185–191.
- R. Croce, T. Morosinotto, S. Castelletti, J. Breton, R. Bassi, The Lhca antenna complexes of higher plants photosystem I, *Biochim. Biophys. Acta* 1556 (2002) 29–40.
- E. Wientjes, R. Croce, The light-harvesting complexes of higher-plant Photosystem I: Lhca1/4 and Lhca2/3 form two red-emitting heterodimers, *Biochem. J.* 433 (2011) 477–485.

- [45] R. Croce, G. Canino, F. Ros, R. Bassi, Chromophore organization in the higher-plant photosystem II antenna protein CP26, *Biochemistry* 41 (2002) 7334–7343.
- [46] I.H.M. van Stokkum, B. van Oort, F. van Mourik, B. Gobets, H. van Amerongen, (Sub)-picosecond spectral evolution of fluorescence studied with a synchroscan streak-camera system and target analysis, *Biophysical Techniques in Photosynthesis*, Springer, 2008. 223–240.
- [47] J.J. Snellenburg, S. Liptonok, R. Seger, K.M. Mullen, I.H.M. van Stokkum, Glotaran: a Java-based graphical user interface for the R package TIMP, *J. Stat. Softw.* 49 (2012).
- [48] I.H.M. van Stokkum, D.S. Larsen, R. van Grondelle, Global and target analysis of time-resolved spectra, *Biochim. Biophys. Acta* 1657 (2004) 82–104.
- [49] I.H.M. van Stokkum, D.S. Larsen, R. van Grondelle, Erratum to “Global and target analysis of time-resolved spectra” [*Biochimica et Biophysica Acta* 1658/2–3 (2004) 82–104], *Biochim. Biophys. Acta* 1658 (2004) 262.
- [50] A.R. Holzwarth, Data analysis of time-resolved measurements, *Biophysical Techniques in Photosynthesis*, Springer, 1996. 75–92.
- [51] K.M. Mullen, I.H.M. van Stokkum, The variable projection algorithm in time-resolved spectroscopy, microscopy and mass spectrometry applications, *Numer. Algorithms* 51 (2009) 319–340.
- [52] J.J. Snellenburg, J.P. Dekker, R. van Grondelle, I.H.M. van Stokkum, Functional compartmental modeling of the photosystems in the thylakoid membrane at 77 K, *J. Phys. Chem. B* 117 (2013) 11363–11371.
- [53] B. van Oort, A. Amunts, J.W. Borst, A. van Hoek, N. Nelson, H. van Amerongen, R. Croce, Picosecond fluorescence of intact and dissolved PSI–LHCI crystals, *Biophys. J.* 95 (2008) 5851–5861.
- [54] K. Broess, G. Trinkunas, A. van Hoek, R. Croce, H. van Amerongen, Determination of the excitation migration time in Photosystem II consequences for the membrane organization and charge separation parameters, *Biochim. Biophys. Acta* 1777 (2008) 404–409.
- [55] K. Gibasiewicz, R. Croce, T. Morosinotto, J.A. Ihalainen, I.H.M. van Stokkum, J.P. Dekker, R. Bassi, R. van Grondelle, Excitation energy transfer pathways in Lhca4, *Biophys. J.* 88 (2005) 1959–1969.
- [56] A.R. Holzwarth, M.G. Muller, J. Niklas, W. Lubitz, Ultrafast transient absorption studies on photosystem I reaction centers from *Chlamydomonas reinhardtii*. 2: mutations near the P700 reaction center chlorophylls provide new insight into the nature of the primary electron donor, *Biophys. J.* 90 (2006) 552–565.
- [57] F. Passarini, E. Wientjes, H. van Amerongen, R. Croce, Photosystem I light-harvesting complex Lhca4 adopts multiple conformations: red forms and excited-state quenching are mutually exclusive, *Biochim. Biophys. Acta* 1797 (2010) 501–508.
- [58] J. Kargul, J. Nield, J. Barber, Three-dimensional reconstruction of a light-harvesting complex I-photosystem I (LHCI-PSI) supercomplex from the green alga *Chlamydomonas reinhardtii*. Insights into light harvesting for PSI, *J. Biol. Chem.* 278 (2003) 16135–16141.
- [59] G. Gulis, K.V. Narasimhulu, L.N. Fox, K.E. Redding, Purification of His6-tagged photosystem I from *Chlamydomonas reinhardtii*, *Photosynth. Res.* 96 (2008) 51–60.
- [60] H. van Amerongen, L. Valkunas, R. van Grondelle, Photosynthetic excitons, *World Sci.* (2000) 401–478.
- [61] E. Wientjes, H. van Amerongen, R. Croce, Quantum yield of charge separation in photosystem II: functional effect of changes in the antenna size upon light acclimation, *J. Phys. Chem. B* 117 (2013) 11200–11208.
- [62] M.G. Muller, J. Niklas, W. Lubitz, A.R. Holzwarth, Ultrafast transient absorption studies on Photosystem I reaction centers from *Chlamydomonas reinhardtii*. 1. A new interpretation of the energy trapping and early electron transfer steps in Photosystem I, *Biophys. J.* 85 (2003) 3899–3922.
- [63] A.R. Holzwarth, M.G. Muller, J. Niklas, W. Lubitz, Charge recombination fluorescence in photosystem I reaction centers from *Chlamydomonas reinhardtii*, *J. Phys. Chem. B* 109 (2005) 5903–5911.
- [64] F.L. de Weerd, J.T. Kennis, J.P. Dekker, R. van Grondelle,  $\beta$ -carotene to chlorophyll singlet energy transfer in the photosystem I core of *Synechococcus elongatus* proceeds via the  $\beta$ -carotene S2 and S1 states, *J. Phys. Chem. B* 107 (2003) 5995–6002.